

**THE EFFECT OF HARD PROTEIN CORONA ON
QD NANOPARTICLE TOWARDS SENESCENT
CELLS**

SEYEDEH PARISA FOROOZANDEHASL

UNIVERSITI SAINS MALAYSIA

2019

**THE EFFECT OF HARD PROTEIN CORONA ON
QD NANOPARTICLE TOWARDS SENESCENT
CELLS**

by

SEYEDEH PARISA FOROOZANDEHASL

Thesis submitted in fulfillment of the requirements
for the degree of
Doctor of Philosophy

August 2019

ACKNOWLEDGEMENT

First and foremost, all praise and thanks is to Allah S.W.T. the Lord of the universe that has given me the strength and opportunity to complete this research. I am heartily thankful to my supervisor Professor, Dr. Azlan Abdul Aziz who was abundantly helpful and offered great assistance, support and guidance. I am extremely grateful to my co-supervisor, Professor, Dr.Morteza Mahmoudi for his valuable guidance through this journey. I would like to express my appreciation to NanoBRI staff, especially Mr. A.S. Navanithan for his guidance.

I owe my deepest gratitude to my beloved parents, for their faith in me, their understanding and endless love and allowing me to be as ambitious as I wanted. It was under their watchful eye that I gained so much drive and an ability to tackle challenges head on.

Lastly, I would like to dedicate this thesis to my beloved mother, Poursan Rezazadeh, who provided me with unfailing support and continuous encouragement throughout my years of study. This thesis would not have been possible without all the sacrifices that my lovely mother has done to enable me to complete my study.

SEYEDEH PARISA FOROOZANDEHASL

School of Physics

Universiti Sains Malaysia

February 2019

TABLE OF CONTENTS

ACKNOWLEDGEMENT	ii
TABLE OF CONTENTS	iii
LIST OF FIGURES	iii
LIST OF TABLES	iii
LIST OF ABBREVIATIONS	iii
ABSTRAK	iii
ABSTRACT	iii
CHAPTER ONE: INTRODUCTION	1
1.1 Overview and rationale of the study	1
1.2 Research objectives	3
1.3 Flow chart of the study	4
CHAPTER TWO: LITERATURE REVIEW	5
2.1 Nanoparticles	5
2.1.1 Characteristics of nanoparticle	5
2.1.2 Nanoparticles in biomedical application	5
2.2 Nanoparticle protein-corona complex	8
2.2.1 Composition of the protein-corona	10
2.2.2 Mechanisms and kinetics of protein adsorption	13
2.2.3 Biological consequences of protein-corona formation on nanoparticles	18
2.3 Cellular uptake pathways of NPs.....	23
2.4 Cellular aging and senescence	29
2.4.1 Characteristic features of senescence	29
2.4.2 Replicative senescence	30
2.4.3 Stress induced premature senescence	32
2.4.3(a) Oxidative stress	32
2.4.3(b) Genotoxic stress	33
2.4.3(c) Oncogene-induced senescence	34
2.4.4 Biomarkers of cellular senescence	34
2.4.4(a) Growth arrest	35
2.4.4(b) Morphology	35

2.4.4(c) Apoptosis resistance	35
2.4.4(d) Gene expression	36
2.4.4(e) Senescence associated- β -galactosidase	36
2.4.4(f) Senescence-associated heterochromatin foci	37
2.4.4(g) Senescence-associated secretory phenotype	37
2.5 Cell death	38
2.5.1 Apoptosis.....	38
2.5.2 Autophagy.....	39
2.5.3 Necrosis	40

CHAPTER THREE: PREPARATION AND CHARACTERIZATION OF NANOPARTICLE-PROTEIN CORONA 42

3.1 Introduction	42
3.2 Materials and Methods	43
3.2.1 Nanoparticle preparation	43
3.2.2 Characterization of nanoparticles	44
3.2.2(a) Transmission electron microscopy (TEM)	44
3.2.2(b) Scanning transmission electron microscope in tandem with energy-dispersive x-ray spectroscopy (STEM-EDX)	44
3.2.2(c) Dynamic light scattering (DLS) and zeta potential measurement.....	44
3.2.2(d) Atomic force microscopy (AFM)	45
3.2.2(e) Fluorescence spectrometry	46
3.2.3 Characterization of hard protein corona	46
3.2.3(a) Sodium dodecyl sulfate polyacrylamide gel electrophoresis (SDS-PAGE)	46
3.2.3(b) Micro bicinchoninic colorimetric (μ BCA) assay	47
3.2.3(c) Matrix assisted laser desorption/ionization–time of flight (MALDI-TOF/TOF) mass spectrometry	47
3.2.3(d) Liquid chromatography tandem mass spectrometry (LC-MS/MS)	48
3.2.4 Statistical analyses	49
3.3 Results and Discussion	50
3.3.1 Size, morphology and elemental analysis of nanoparticles	50
3.3.2 Size separation, estimation and identification of protein corona	53

3.3.3 Nanoparticle size distribution and agglomeration analysis	61
3.3.4 Nanoparticle gravitational sedimentation analysis	75
3.3.5 Nanoparticle photostability analysis	81
3.4 Conclusion	86

**CHAPTER FOUR: CELL CULTURING, MAINTENANCE AND INDUCTION
OF CELLULAR SENESCENCE 87**

4.1 Introduction	87
4.2 Materials and methods	89
4.2.1 Cell culture	89
4.2.1(a) Normal human lung fibroblast (IMR90)	89
4.2.1(b) Normal human colon epithelial (CCD841CoN)	89
4.2.1(c) Untransformed adult human lung fibroblasts (AG02262).....	89
4.2.1(d) Untransformed adult human lung fibroblasts (AG02603)	90
4.2.1(e) Untransformed fetal human lung fibroblasts (AG04450)	90
4.2.2 Senescence induction of IMR90 and CCD841CoN cells	90
4.2.2(a) Replicative senescence	90
4.2.2(b) Genotoxic stress induced premature senescence	91
4.2.2(c) Oxidative stress induced premature senescence	91
4.2.3 Cellular senescence biochemical characterization	92
4.2.3(a) 5-bromo-2'-deoxyuridine (BrdU) incorporation assay	92
4.2.3(b) Senescence associated β -galactosidase (SA- β -Gal) assay	93
4.2.3(c) Senescence associated heterochromatin foci (SAHF) assay	94
4.2.4 Statistical analyses	95
4.3 Results and Discussion	96
4.3.1 Population doubling level to reach deep senescence	96
4.3.1(a) Cell growth profile	96
4.3.1(b) BrdU incorporation assay analysis	100
4.3.1(c) SA- β -Gal assay analysis	102
4.3.1(d) SAHF assay analysis	104
4.3.2 Effective concentration of doxorubicin (DOX) and hydrogen peroxide (H ₂ O ₂) for cell aging	106
4.3.2(a) Cell growth profile	109
4.3.2(b) BrdU incorporation assay analysis	118
4.3.2(c) SA- β -Gal assay analysis	124

4.3.2(d) SAHF assay analysis	130
4.3.3 Comparative analysis of cell aging methods.....	136
4.3.4 Aging biomarker analysis in primary fibroblast cells.....	144
4.4 Conclusion	148
CHAPTER FIVE: LIVE IMAGING OF CELL-NANOPARTICLE INTERACTION	149
5.1 Introduction	149
5.2 Materials and methods	150
5.2.1 Energy dependent cell uptake assay.....	150
5.2.2 Endocytic cell uptake assay	151
5.2.3 Exocytosis imaging	152
5.2.4 Colocalization imaging	152
5.2.5 Statistical analyses	153
5.3 Results and Discussion	154
5.3.1 Energy dependent cell uptake of nanoparticles	154
5.3.2 Endocytic cell uptake of nanoparticles	162
5.3.3 Exocytosis of nanoparticles	167
5.3.4 Surface specific cell uptake of nanoparticles	174
5.3.5 Localization of nanoparticles within cell	181
5.4 Conclusion	189
CHAPTER SIX: <i>IN VITRO</i> CYTOTOXICITY OF NANOPARTICLES	191
6.1 Introduction	191
6.2 Materials and methods	192
6.2.1 WST-1 cell viability assay	192
6.2.2 Neutral red retention (NRR) assay	192
6.2.3 Lactate dehydrogenase (LDH) release assay	193
6.2.4 Lysosomal alkalization	197
6.2.5 Volume of acidic compartment (VAC) measurement	197
6.2.6 Cadmium toxicity.....	198
6.2.7 Derivative toxicity due to nanoparticle leaching and disintegration	198
6.2.8 Autophagy and apoptosis inhibitor treatment of cells	199
6.2.9 Statistical analyses	199
6.3 Results and Discussion	200

6.3.1 Acute cytotoxic effects of nanoparticles	200
6.3.2 Effect of protein corona on nanoparticle toxicity	209
6.3.3 Effect of cell size on nanoparticle toxicity	212
6.3.4 Modality and mechanism of senescent cell death induced by nanoparticles .	203
6.4 Conclusion	246
CHAPTER SEVEN: SUMMARY	247
7.1 General conclusion	247
7.2 Suggestions for future studies	251
REFERENCES	252
LIST OF PUBLICATIONS	282

LIST OF FIGURES

		Page
Figure 2.1	The nanoparticle–corona complex in a biological environment. (a) It is the nanoparticle–corona complex, rather than the bare nanoparticle, that interacts with biological machinery, here with a cell membrane receptor. (b) Relevant processes (arrows), in both directions (on/off), for a nanoparticle interacting with a receptor.	9
Figure 2.2	Entry of NPs into cell using different endocytotic pathways. A) Macropinocytosis and phagocytosis. B) Clathrin-mediated endocytosis, clathrin-caveolin independent endocytosis and caveolae-mediated endocytosis.	28
Figure 2.3	Features of senescent cells: Several markers were identified to characterize the senescent state in relation to morphology and proteostasis	30
Figure 3.1	(A) TEM image and (B) size distribution of QD-PEG NPs. (C) TEM image and (D) size distribution of QD-HC NPs. (E) HRTEM image of QD-PEG nanoparticles encircled in red and (F) EDX spectrum of QD-PEG.	52
Figure 3.2	(A) BSA standard curve and (B) mass of adsorbed proteins at increasing concentration of nanoparticles.	56
Figure 3.3	SDS-PAGE analysis of hard protein corona formed on QD-HC nanoparticles: (A) coomassie blue staining, (B) silver staining and (C) comparison between the staining methods in identifying low abundance proteins/peptides.	57
Figure 3.4	MALDI-TOF/TOF analysis of the four most abundant hard protein corona (A-D) formed on QD-HC nanoparticles.	58
Figure 3.5	Hypothetical schematic illustration of QD-PEG nanoparticle transformation in 55% human plasma solution	60
Figure 3.6	Colloidal stability of QD-PEG and QD-HC nanoparticles at various concentrations in DPBS solution. (A) Intensity based DLS	64

	measurement, (B) PdI measurement and (C) zeta potential measurement.	
Figure 3.7	Colloidal stability of 30 nM QD-PEG nanoparticles at various incubation period in serum free cell culture medium. (A) Intensity based DLS measurement, (B) PdI measurement and (C) zeta potential measurement.	67
Figure 3.8	Colloidal stability of 30 nM and 45 nM QD-HC nanoparticles at various incubation period in serum free cell culture medium. (A) Intensity based DLS measurement, (B) PdI measurement and (C) zeta potential measurement.	68
Figure 3.9	Colloidal stability of 30 nM QD-PEG nanoparticles at 60 min incubation period in serum free and preconditioned cell culture medium. (A) Intensity based DLS measurement, (B) PdI measurement and (C) zeta potential measurement.	72
Figure 3.10	Colloidal stability of 30 nM and 45 nM QD-HC nanoparticles at 60 min incubation period in serum free and preconditioned cell culture medium. (A) Intensity based DLS measurement, (B) PdI measurement and (C) zeta potential measurement.	73
Figure 3.11	Hypothetical schematic illustration of nanoparticle's aggregation models. (A) homoaggregation among QD-PEG NPs, (B) homoaggregation among QD-HC NPs and (C) heteroaggregation between QD-PEG NPs and extracellular proteins.	74
Figure 3.12	Comparison of mean size of individual QD-PEG and QD-HC nanoparticle sediments after (A) 30min and (B) 90 min of incubation in cell culture medium.	77
Figure 3.13	Microscopic images of QD-PEG NPs (left) and its corresponding AFM scans (right).	78
Figure 3.14	AFM images and height profiles of 30nm QD-PEG pertaining to gravitational sedimentation size after 90 minutes of incubation time in cell culture medium.	79
Figure 3.15	AFM images and height profiles of 30nm QD-PEG pertaining to gravitational sedimentation size after 30 minutes of incubation time in cell culture medium.	80

Figure 3.16	Photostability of QD-PEG and QD-HC at cell cytosolic and lysosomal pH after 4 hours of incubation.	84
Figure 3.17	Hypothetical schematic illustration of QD-HC nanoparticle gradual disintegration in ALF/protease solution.	85
Figure 4.1	Flow chart illustrating the cell aging methods deployed in the current study	88
Figure 4.2	(A) Growth curve of IMR90 cells. Morphology of cells at (B) rapid proliferation phase (C) deep senescence phase.	98
Figure 4.3	(A) Growth curve of CCD841CoN cells. Morphology of cells at (B) rapid proliferation phase (C) deep senescence phase.	99
Figure 4.4	Quantification of proliferating cells in (A) IMR90 and (B) CCD841CoN cultures at different population doubling levels.	101
Figure 4.5	Quantification of SA- β -galactosidase expression in (A) IMR90 and (B) CCD841CoN cells at different population doubling levels.	103
Figure 4.6	Quantification of SAHF formation in (A) IMR90 and (B) CCD841CoN cells at different population doubling levels.	105
Figure 4.7	Toxicity graph of (A) hydrogen peroxide and (B) doxorubicin treatment on young IMR90 and CCD841CoN cells.	108
Figure 4.8	(A) Growth curve of IMR90 cells after exposure to hydrogen peroxide treatments at different concentrations. Morphology of cells at (B) 10 μ M, (C) 30 μ M, and (D) 50 μ M hydrogen peroxide treatments.	111
Figure 4.9	(A) Growth curve of CCD841CoN cells after exposure to hydrogen peroxide treatments at different concentrations. Morphology of cells at (B) 10 μ M, (C) 30 μ M, and (D) 50 μ M hydrogen peroxide treatments.	113
Figure 4.10	(A) Growth curve of IMR90 cells after exposure to doxorubicin treatments at different concentrations. Morphology of cells at (B) 40nM, (C) 70nM, and (D) 100nM doxorubicin treatments.	115
Figure 4.11	(A) Growth curve of CCD841CoN cells after exposure to doxorubicin treatments at different concentrations. Morphology of cells at (B) 40nM, (C) 70nM, and (D) 100nM doxorubicin treatments.	117

Figure 4.12	Quantification of proliferating cells in (A) IMR90 and (B) CCD841CoN cultures after treatment with different concentrations of hydrogen peroxide.	120
Figure 4.13	Quantification of proliferating cells in (A) IMR90 and (B) CCD841CoN cultures after treatment with different concentrations of doxorubicin.	123
Figure 4.14	Quantification of SA- β -galactosidase expression in (A) IMR90 and (B) CCD841CoN cells after treatment with different concentrations of hydrogen peroxide.	126
Figure 4.15	Quantification of SA- β -galactosidase expression in (A) IMR90 and (B) CCD841CoN cells after treatment with different concentrations of doxorubicin.	129
Figure 4.16	Quantification of SAHF formation in (A) IMR90 and (B) CCD841CoN cells after treatment with different concentrations of hydrogen peroxide.	132
Figure 4.17	Quantification of SAHF formation in (A) IMR90 and (B) CCD841CoN cells after treatment with different concentrations of doxorubicin.	135
Figure 4.18	Effects of senescence induction on cell proliferation. Fluorescence micrograph of (A) IMR90 cells, (B) CCD841CoN cells and (C) quantification of cell proliferation.	138
Figure 4.19	Effects of senescence induction on SA- β -galactosidase expression. Bright field micrograph of (A) IMR90 cells, (B) CCD841CoN cells and (C) quantification of SA- β -galactosidase expression.	140
Figure 4.20	Effects of senescence induction on SAHF formation. Fluorescence micrograph of (A) IMR90 cells, (B) CCD841CoN cells and (C) quantification of SAHF formation.	142
Figure 4.21	(A) Fluorescence micrograph and (B) quantification of cell proliferation in primary fibroblast cells.	145
Figure 4.22	(A) Bright field micrograph and (B) quantification of SA- β -galactosidase expression in primary fibroblast cells.	146
Figure 4.23	(A) Fluorescence micrograph and (B) quantification of SAHF formation in primary fibroblast cells.	147

Figure 5.1	Internalization of QDs in (A) IMR90 and (B) CCD841CoN cells cultured at different temperatures and endocytic inhibitors.	157
Figure 5.2	Fluorescence micrographs of young and senescent (A) IMR90 cells and (B) CCD841CoN cells.	159
Figure 5.3	Cell size of IMR90 and CCD841CoN cells at different states.	161
Figure 5.4	Internalization of QDs in (A) IMR90 cells and (B) CCD841CoN cells pre-treated with endocytic inhibitors, monodansylcadaverine (MDC) and nystatin that targets clathrin dependent pathway and caveolae dependent pathway, respectively.	164
Figure 5.5	Fluorescence micrographs of QDs uptake in young and senescent IMR90 and CCD841CoN cells that were pretreated with nystatin.	166
Figure 5.6	Fluorescence micrographs of QDs exocytosis in (A) replicating IMR90 cells, (B) replicating CCD841CoN cells, (C) contact inhibited IMR90 cells, and (D) contact inhibited CCD841CoN cells	168
Figure 5.7	Fluorescence micrographs of QDs exocytosis from senescent IMR90 cells in a time course experiment.	169
Figure 5.8	Fluorescence micrographs of QDs exocytosis from senescent CCD841CoN cells in a time course experiment.	170
Figure 5.9	(A) Exocytosis of QDs from young IMR90 and CCD841CoN cells after 1.5 hours of incubation. (B) Exocytosis of QDs from senescent IMR90 and CCD841CoN cells after 4 hours of incubation.	173
Figure 5.10	Internalization of QDs in (A) IMR90 cells and (B) CCD841CoN cells cultured with and without 15% FBS.	180
Figure 5.11	Fluorescence micrographs of QDs colocalization in lysosomes of young IMR90 and CCD841CoN cells.	183
Figure 5.12	Fluorescence micrographs of QDs colocalization in lysosomes of senescent IMR90 and CCD841CoN cells.	184
Figure 5.13	Fluorescence micrographs of lysosomes in young and senescent (A) IMR90 cells and (B) CCD841CoN cells.	185
Figure 5.14	(A) Monochromatic fluorescent micrograph depicting Hoechst 33342 stained nucleus of IMR90 senescent cell. The nucleus was marked as (N) and the arrows depict lipofuscin pigments. (B)	187

	Monochromatic fluorescent micrograph portraying localization of quantum dots (red circle) within the senescent cells. (C) Merged fluorescent image of stained nucleus (blue) and quantum dots (red) in pseudocolours, marked as N and QD, respectively.	
Figure 5.15	Monochromatic fluorescent micrograph depicting Hoechst 33342 stained nucleus of (A) young and (B) senescent IMR90 cells.	188
Figure 6.1	Cell titration curve for WST-1 assay of (A) IMR90, (B) CCD841CoN, and (C) primary fibroblast cells.	194
Figure 6.2	Cell titration curve for NRR assay of (A) IMR90 and (B) CCD841CoN cells.	195
Figure 6.3	Cell titration curve for LDH assay of (A) IMR90 and (B) CCD841CoN cells.	196
Figure 6.4	Acute cytotoxicity of QD nanoparticles on (A) young IMR90 cells, (B) young CCD841CoN cells and (C) primary fibroblast cells of different age groups.	204
Figure 6.5	Acute cytotoxicity of QD nanoparticles on senescent (A) IMR90 cells and (B) CCD841CoN cells. (C) IC ₅₀ values of nanoparticles on senescent IMR90 and CD841CoN cells.	206
Figure 6.6	Comparison of QD nanoparticles toxicity on senescent (A) IMR90 and (B) CCD841CoN cells.	208
Figure 6.7	Flow chart summarizing the possible permutations of the cytotoxicity results and the effect of protein corona within this scheme.	211
Figure 6.8	Fluorescence micrographs of (A) senescent IMR90 cells, (B) folded senescent IMR90 cells, (C) senescent CCD841CoN cells, and (D) folded senescent CCD841CoN cells.	215
Figure 6.9	(A) Temporal analysis and (B) quantification of QD nanoparticle toxicity on normal and folded senescent IMR90 cells.	216
Figure 6.10	(A) Temporal analysis and (B) quantification of QD nanoparticle toxicity on normal and folded senescent CCD841CoN cells.	217
Figure 6.11	Temporal analysis of QD nanoparticles toxicity on senescent IMR90 cells with (A) 30 nM QD-PEG and (B) 45 nM QD-HC. Toxicity measurement was performed using WST-1 colorimetric assay, neutral red retention (NRR) assay and lactate dehydrogenase (LDH)	220

assay after 24h incubation. H₂O₂: hydrogen peroxide, DOX: doxorubicin. Data are represented as mean ± SD. n=6 for each group.

- Figure 6.12 Temporal analysis of QD nanoparticles toxicity on senescent CCD841CoN cells with (A) 30 nM QD-PEG and (B) 45 nM QD-HC. Toxicity measurement was performed using WST-1 colorimetric assay, neutral red retention (NRR) assay and lactate dehydrogenase (LDH) assay after 24h incubation. H₂O₂: hydrogen peroxide, DOX: doxorubicin. Data are represented as mean ± SD. n=6 for each group. 221
- Figure 6.13 (A) Fluorescence micrographs of lysosomal membrane permeabilization in senescent IMR90 cell due to QD toxicity. (B) Fluorescence micrographs of QD toxicity on senescent IMR90 cell. Micrographs are ordered from (a-i) to correspond with the progression of incubation time. Release of QD nanoparticles from cell due to plasma membrane leakage indicates necrotic cell death. Experiments were carried out at 37°C for 24h. Cells were stained with CMFDA CellTracker fluorescent dye (green), lysosomes were stained with LysoTracker Blue fluorescent dye (blue) and QD-PEG nanoparticles were marked in red. Bar = 50µm. 225
- Figure 6.14 (A) Fluorescence micrographs of lysosomal membrane permeabilization in senescent CCD841CoN cells due to QD toxicity. (B) Fluorescence micrographs of QD toxicity on senescent CCD841CoN cells. Micrographs are ordered from (a-i) to correspond with the progression of incubation time. Release of QD nanoparticles from cell due to plasma membrane leakage indicates necrotic cell death. Experiments were carried out at 37°C for 24h. Cells were stained with CMFDA CellTracker fluorescent dye (green), lysosomes were stained with LysoTracker Blue fluorescent dye (blue) and QD-PEG nanoparticles were marked in red. Bar = 50µm. 227
- Figure 6.15 (A) Temporal analysis and (B) quantification of QD nanoparticle toxicity on normal and ammonium chloride pre-treated senescent IMR90 cells. 228

Figure 6.16	(A) Temporal analysis and (B) quantification of QD nanoparticle toxicity on normal and ammonium chloride pre-treated senescent CCD841CoN cells.	229
Figure 6.17	Lysosomal content of young and senescent IMR90 and CCD841CoN cells.	232
Figure 6.18	(A) Temporal analysis and (B) quantification of cadmium and QD supernatant toxicity on normal and inhibitor pre-treated senescent IMR90 cells. ZVAD-FMK and 3-MA are inhibitors of apoptosis and autophagy, respectively.	237
Figure 6.19	(A) Temporal analysis and (B) quantification of cadmium and QD supernatant toxicity on normal and inhibitor pre-treated senescent CCD841CoN cells.	238
Figure 6.20	Fluorescence micrographs of senescent CCD841CoN cells undergoing autophagic cell death due to nanoparticle exposure.	240
Figure 6.21	Cell viability of young IMR90 and CCD841CoN cells treated with cadmium chloride.	245

LIST OF TABLES

		Page
Table 3.1	LC-MS/MS results of ten most abundant hard protein corona formed on QD-HC NPs.	59
Table 4.1	Comparison of data from different cell senescence induction methods.	137
Table 6.1	Cytotoxic effect of nanoparticles on young, senescent and primary cells.	203

LIST OF ABBREVIATIONS

AFM	Atomic force microscopy
ALF	Artificial lysosomal fluid
ATP	Adenosine triphosphate
SDS-PAGE	Sodium dodecyl sulfate polyacrylamide gel electrophoresis
μ BCA	Micro bicinchoninic colorimetric assay
MALDI-TOF/TOF	Matrix assisted laser desorption/ionization–time of flight
LC-MS/MS	Liquid chromatography tandem mass spectrometry
BrdU	5-bromo-2'-deoxyuridine
SA- β -Gal	Senescence associated β -galactosidase
SAHF	Senescence associated heterochromatin foci
DOX	Doxorubicin
H ₂ O ₂	Hydrogen peroxide
NRR	Neutral red retention
LDH	Lactate dehydrogenase
VAC	Volume of acidic compartment
CO ₂	Carbon dioxide
PEG	Polyethylene glycol
HRTEM	High-resolution transmission electron microscopy
FBS	Fetal Bovine Serum
PDL	Population doubling level
MDC	Monodansylcadaverine
PBS	Phosphate buffered saline
NaN ₃ + 2DG	Sodium azide + 2-deoxyglucose
ROS	Reactive oxygen species
3-MA	3-Methyladenine

KESAN PROTEIN KERAS KORONA PADA NANOPARTIKEL QD TERHADAP SEL PENUAAN

ABSTRAK

Perubatan nano merupakan bidang kajian penting yang mengkaji penggunaan bahan nano dan nanopartikel dalam terapi perubatan dan tujuan diagnostik. Walaubagaimanapun, tidak banyak kajian yang menumpukan pada aspek penuaan yang berkaitan dengan nanomedikal yang mungkin berguna untuk merawat penyakit yang berkaitan dengan penuaan seperti sindrom Werner, sarcopenia dan Alzheimer. Dalam kerja ini, potensi sitotoksik titik kuantum (QD-PEG) dan QD-PEG bersalut protein keras corona (QD-HC) pada sel-sel yang berbeza umur diperiksa. Pada fasa awal kajian, interaksi QD dengan protein dari plasma darah manusia dianalisis. Keputusan telah menunjukkan bahawa corona protein dapat membentuk pada QD-PEG berdasarkan analisis SDS-PAGE, MALDI-TOF/TOF, LC-MS/MS dan μ BCA. Pembentukan corona protein keras mengubahsui sifat fizikokimia QD-PEG berdasarkan analisis TEM, AFM, DLS dan potensi zeta. Telah ditentukan bahawa perubahan kepada sifat-sifat fiziokimia telah menjejaskan keupayaan koloid QD-PEG secara signifikan. Pada tahap berkadar konsentrasi nanopartikel, corona protein keras telah memberi ciri-ciri fotonik dan koloid yang unik kepada QD-PEG yang lebih bersesuaian untuk aplikasi nanomedikal dari segi: (1) dipertingkatkan kestabilan fotonik dalam keadaan pH yang terlampau, (2) rintangan yang lebih besar kepada perubahan dalam medium extracellular yang mendorong penumpuan dan pemendapan graviti, dan (3) meningkatkan keteguhan QD-PEG daripada kemusnahan dan larut lesap bahan terasnya dalam keadaan pH yang terlampau. Dalam fasa kedua kajian, kaedah penuaan yang berbeza telah digunakan untuk

membangunkan model senescent sel fibroblast (IMR90) dan sel epitelium (CCD841CoN). Hasilnya telah menunjukkan bahawa model senescent untuk sel IMR90 dan sel CCD841CoN telah berjaya dibangunkan. Dalam fasa akhir kajian ini, potensi sitotoksik daripada QDs pada sel-sel muda dan uzur dinilai menggunakan ujian WST-1, NRR dan LDH. Keputusan daripada kajian menunjukkan bahawa QDs tidak akut toksik kepada sel muda IMR90 dan sel muda CCD841CoN. Sebaliknya, QDs memberi kesan toksik kepada sel-sel senescent IMR90 dan CCD841CoN dengan tahap yang berbeza pada masa pendedahan yang sama. Data telah menunjukkan bahawa kesan toksik QD-PEG telah menyebabkan kematian nekrotik kepada sel senescent IMR90 dan CCD841CoN melalui permeabilisasi membran lysosom dalam tempoh 24 jam inkubasi. Sel-sel senescent mempunyai tindak balas yang berbeza terhadap kesan-kesan toksik disebabkan oleh QD-HC bergantung kepada kepekannya. Pada kepekatan QD-PEG yang sama, QD-HC telah menyebabkan kematian sel senescent IMR90 dan CCD841CoN melalui autophagy; manakala pada kepekatan QD-HC yang lebih tinggi, kematian sel secara nekrotik melalui permeabilisasi membran lysosom diperhatikan dalam tempoh 24 jam inkubasi. Penemuan kajian ini akan memberi manfaat kepada para penyelidik dalam bidang perubatan nano untuk merancang eksperimen mereka dengan lebih berkesan selepas menyesuaikan pengaruh protein korona dan perbezaan usia dalam kajian yang memaparkan sistem penyampaian ubat berasaskan nanopartikel yang ditujukan kepada aplikasi terapeutik atau klinikal.

THE EFFECT OF HARD PROTEIN CORONA ON QD NANOPARTICLE TOWARDS SENESCENT CELLS

ABSTRACT

Nanomedicine is an important area of study that examines the utilization of nanomaterials and nanoparticles in medical therapy and diagnostic purposes. However, not many studies have focused on the aging related aspect of nanomedical research that could have been valuable in treating aging associated diseases such as Werner syndrome, sarcopenia and Alzheimer's. In the present work, the cytotoxic potential of PEGylated quantum dots (QD-PEG) and hard protein corona coated QD-PEG (QD-HC) on cells of opposing age groups were examined. In the initial phase of the study, the interaction of QDs with proteins from human blood plasma were analyzed. The results have shown that protein corona was able to form on pristine QD-PEG based on SDS-PAGE, MALDI-TOF/TOF, LC-MS/MS and μ BCA analysis. Formation of hard protein corona had transformed its physicochemical properties, which had in turn affected the colloidal stability of QD-PEG in a significant manner. At proportionate levels of nanoparticle concentration, hard protein corona had imbued distinct photonic and colloidal characteristics to QD-PEG that were better suited for nanomedical applications in terms of: (1) enhanced photostability at extreme pH conditions, (2) greater resistance to changes in extracellular medium that induces agglomeration and gravitational sedimentation, and (3) increased robustness to degradation and leaching of QDs' core materials at extreme pH conditions. In the second phase of the study, different aging methods were employed to develop senescent models of fibroblast (IMR90) and epithelial (CCD841CoN) cells. Based on the benchmarks established in the current experiment, senescent models for

IMR90 and CCD841CoN cells were successfully developed. In the final phase of the study, the cytotoxic potential of the QDs on young and senescent cells were assessed and results from the study have demonstrated that the QDs were not acutely toxic on the former. In contrast, the QDs were lethal to senescent cells of both types with varying degree at the same exposure time. The data have shown that QD-PEG were acutely toxic to senescent IMR90 and CCD841CoN cells, leading to lysosomal membrane permeabilization induced necrotic cell death. The senescent cells had divergent response to the toxic effects induced by QD-HC depending on its concentration. At similar concentration of QD-PEG, QD-HC had induced autophagic cell death due to cadmium toxicity and halved the senescent cell population; while, at much higher concentrations of QD-HC, lysosomal membrane permeabilization induced necrosis was observed, resulting in total death of senescent cell population. At all instances, the common denominator was the disruption to the lysosomal activity of senescent cells preceding the loss of its viability. Incidentally, QD disintegration within the lysosomal compartment was determined to be the precursor event leading up to the binary cell deaths. The rate of QD disintegration was the determining factor for the mode of cell death and protein corona was found to effect this process significantly. Deeper introspection has led to the discovery that protein corona had delayed the QDs' disintegration and consequently had attenuated its cytotoxic potential. The susceptibility of senescent cells to the toxic effects of QDs were attributed to the deterioration of its organelles and disruption in cellular functions relative to the young phenotype. The current findings will benefit researchers in the field of nanomedicine to design their experiments more effectively after adjusting for protein corona influences and age related differences in studies featuring nanoparticle based drug delivery systems geared towards therapeutic or clinical applications.

CHAPTER ONE: INTRODUCTION

1.1 Overview and rationale of the study

The field of nanomedicine is expanding at an astounding rate largely due to the amalgamation of technology from other emerging fields such as nanotechnology, biotechnology and bioconjugation chemistry. The core component of this innovative technology is nanoparticle and its subsequent utility as therapeutic and diagnostic agents in clinical applications makes it an active area of research.

Quantum dots (QDs) are a class of nanoparticle that are widely being used in the biomedical field for diagnostic and imaging applications. Controlled illumination, enhanced resolution and greater resistance to photobleaching relative to the conventional stains are some of the qualities that made QDs an invaluable tool in live imaging of small animals and humans. The delivery of these QDs were mostly administered intravenously at the target site and tracked throughout the circulatory system in the body. As a consequence, the QDs will encounter blood plasma proteins that adsorb onto the circulating nanoparticles either reversibly or irreversibly depending on the affinity of the proteins to the nanoparticle. This phenomenon of protein adsorption is known as ‘The Vroman Effect’ and the adsorbing proteins are denoted as protein corona (Lesniak *et al.*, 2012; Mahmoudi, 2018). Ultimate manifestation of the interaction between these two entities is the modification of QD’s physicochemical properties. This is an undesirable outcome as the QDs are essentially tailored to perform specific functions such as targeted entry into the cells and even targeted sites within the cells or organelles. As such, methods

to circumvent this effect or incorporate it as part of the delivery strategy will greatly benefit in increasing the targeting yield and efficacy of the QDs while inadvertently improving its imaging resolution. In the first phase of this study, the interaction of QDs with proteins from human blood plasma were analysed.

Another serious consideration when administering QDs to living organisms are its toxic effects on the cell, which creates a potential liability for its use. QDs can be toxic to cells due to intrinsic factors such as its core chemical composition, surface chemistry, size distribution and colloidal stability. To study the toxic effects and optimize the parameters for safe administration of QDs, *in vitro* cellular models can be utilized. These *in vitro* models are useful tools to quantitatively study the toxic effect of nanoparticles on different types of cultured cells. Apart from the potential of QDs to induce deleterious effects on the cells, the cellular model selected for cytotoxicity evaluation may have an impact on the final outcome of the study.

Some of the cellular models that were typically employed for cytotoxicity testing of nanoparticles are fibroblast, epithelial, endothelial, macrophage, cancer and stem cells. The prerequisite for selecting the *in vitro* cellular models is to ideally represent the *in vivo* conditions. However, the age of the cell is an overlooked factor in many studies and the interaction of nanoparticles with ageing cells were rarely addressed, if any in the cytotoxicity studies. By using senescent cell models along with the non-senescent cells of similar genotype, the conclusion of the study will epitomize heterogeneity and reduced

biasness. Therefore, age related studies will provide a more comprehensive understanding of nanoparticle toxicity as it reflects the diversity in the general population. In the second phase of the study, senescent models of fibroblast and epithelial cells were developed using established cell ageing methods to assess the cytotoxic potential of QDs.

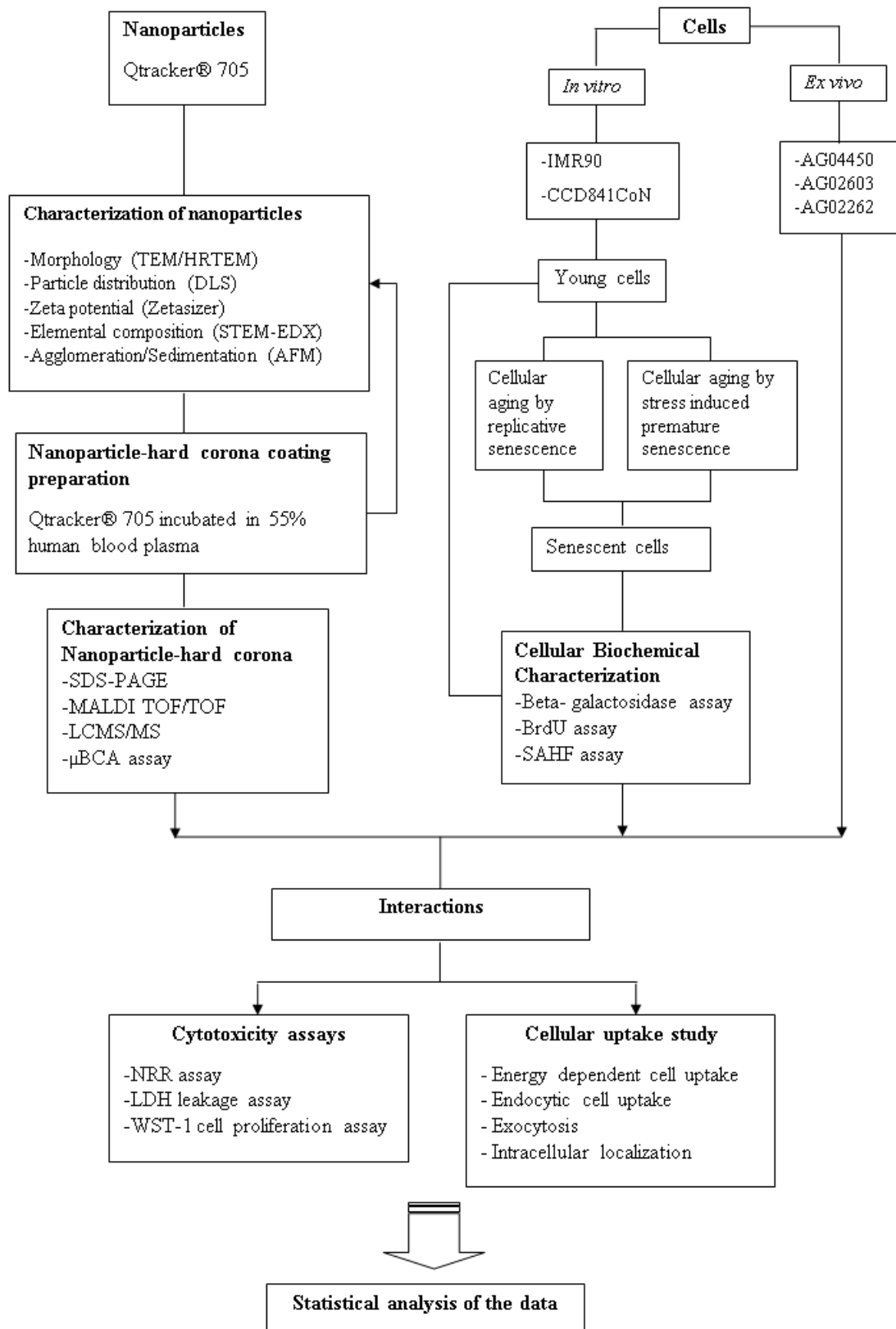
Principal goal of the current study was to gauge the effect of protein corona formation on QDs and its subsequent correspondence with cells of different age groups in an *in vitro* setting. Thus, the two tiered experimental approach discussed above were integrated in the final part of the study and the resulting data were meticulously evaluated.

1.2 Research objectives

The current study was undertaken with the following objectives:

1. To characterize and evaluate the impact of hard protein corona on the physicochemical properties of the quantum dots.
2. To establish *in vitro* senescent cell models using fibroblast (IMR90) and epithelial (CCD841CoN) cells.
3. To determine the interaction and cytotoxic potential of pristine and hard corona coated quantum dots on young and senescent cells.
4. To investigate the modality and mechanism of senescent cell death induced by the quantum dots.

1.3 Flow chart of the study



CHAPTER TWO: LITERATURE REVIEW

2.1 Nanoparticles

2.1.1 Characteristics of nanoparticle

Nanoparticles (NPs) are defined as particles with all its three dimensions confined within the range of 1 to 100 nm (Albanese *et al.*, 2012; Docter *et al.*, 2015a; Bhatia, 2016). The growing attention to NP stem from the fact that their mechanical, chemical, optical electrical, and magnetic properties differs to those of bulk counterparts and these properties can be altered by varying the size (Mahmoudi *et al.*, 2011a; Rahman *et al.*, 2013). Due to their capability of tuning properties for intended requirements, NPs are of significant interest in different fields such as physics, chemistry, engineering, electronics, and biology (Aggarwal *et al.*, 2009; Mahmoudi *et al.*, 2011a; Kharazian *et al.*, 2016; Schöttler *et al.*, 2016). Nanoparticles can be made of inorganic materials like gold, silica, iron oxide, or made of organic polymers including polystyrene (PS), poly (lactic-co-glycolic acid) (PLGA) and polylactic acid (PLA) (Schöttler *et al.*, 2016).

2.1.2 Nanoparticles in biomedical application

The utilization of NPs in biomedical application arise from their inherent properties of small size and high surface to volume ratio (Chinen *et al.*, 2015; Smith *et al.*, 2015). Small size of NP enables them to translocate cross biological barriers and reach subcellular compartment, biological components and those targets that were not possible to access previously such as brain (Saptarshi *et al.*, 2013; Caracciolo *et al.*, 2016). In particular, NPs smaller than 100 nm are able to enter the cells, smaller than 40 nm enter

nucleus of the cells and less than 35 nm can cross the blood brain barrier (Dawson *et al.*, 2009). Moreover, high surface to volume ratio of NP make them highly active and more efficiently in interactions with biological component than that of bulk counterpart (Karmali and Simberg, 2011; Westmeier *et al.*, 2015; Polyak and Cordovez, 2016). These interesting properties of nanoparticles make them as a promising multifunctional tool in different medical applications (Docter *et al.*, 2015a).

Nanoparticles are increasingly considered to employ in medical imaging, drug delivery, diagnostic, and hyperthermic therapy purposes (Rahman *et al.*, 2013; Mahmoudi, 2016). Likewise, nanoparticles are highly potential to use as contrast agent in magnetic resonance imaging (MRI), fluorescence spectroscopy and optical imaging (Seeney *et al.*, 2012; Hou *et al.*, 2013; Rizzo *et al.*, 2013; Westmeier *et al.*, 2015). Metal oxides have begun to use in magnetic resonance imaging in 1970s (Rahman *et al.*, 2013). Magnetic nanoparticles have been widely used in magnetic resonance imaging, magnetic particle imaging and magnetic drug targeting as well as in hyperthermia application (Krishnan, 2010; Gräfe *et al.*, 2016). Plasmonic particles such as gold (Au) and silver (Ag) are employed for optical imaging along with laser induced photothermal therapy (de Aberasturi *et al.*, 2015).

Nanoparticles have demonstrated promising features for the delivery of therapeutic drugs to the target site of body (Mirshafiee *et al.*, 2013). In contrast to micron-sized particles that rapidly eliminated by immune system, nanoparticles in drug delivery system can be delivered to all organs (Mause and Weber, 2010; Rak, 2010; Lee *et al.*, 2015). Moreover, NP-based drug delivery shows higher solubility, improved

pharmacokinetics, reduced toxicity, greater biodistribution and increased drug bioavailability which result in fewer side effects and enhancing therapeutic index of drugs (Pautler and Brenner, 2010; Wahajuddin, 2012; Polyak and Cordovez, 2016).

Administration of NP in drug delivery has opened up new opportunities in cancer therapy (van der Meel *et al.*, 2013; Pearson *et al.*, 2014a). Encapsulation of drugs in nanoparticles carrier or nanocapsules have been introduced in cancer therapy as a new promising approach (Albanese *et al.*, 2012; Salvati *et al.*, 2013; Mirshafiee *et al.*, 2016a). Severe side effects that cause by chemotherapeutic drugs due to their high cytotoxicity can be diminished by utilizing nanocarriers. Among chemotherapeutic drugs doxorubicin and paclitaxel were the first drugs which was administrated by nanocarriers (Schöttler *et al.*, 2016).

Numerous nanotherapeutics have already acknowledged clinical approval and several others are currently going through clinical trials (Wolfram *et al.*, 2014). Thus, due to increase application of nanoparticles in nanomedicine, it is crucial to understand their interaction with biological compartment and consequent physiological response to ensure the safe and efficient implementation of nanomedicine (Nel *et al.*, 2009; Mahmoudi *et al.*, 2011b; Walkey and Chan, 2012).

2.2 Nanoparticle protein-corona complex

Due to their large surface to volume ratio, nanoparticles in biological medium tend to lower their high surface energy by interacting with medium components (Monopoli *et al.*, 2011a; Wolfram *et al.*, 2014; Polyak and Cordovez, 2016; Westmeier *et al.*, 2016). Therefore, when NP is dispersed in biological medium physical and chemical interactions arise, leading to formation of new interface between NP and biological component called “bio-nano interface” which is merging of organic and synthetic worlds (Mahmoudi *et al.*, 2011a; Treuel and Nienhaus, 2012; Gunawan *et al.*, 2014; Schöttler *et al.*, 2016). It is now well accepted that upon introduction of NP to biological environment, variety of proteins would cover the surface of NP forming a layer, called “protein corona” (Treuel, 2013; Pearson *et al.*, 2014b; Pozzi *et al.*, 2015; Corbo *et al.*, 2016; Mahmoudi, 2016).

It is noteworthy to mention that it is protein corona that primarily interact with biological component rather than the pristine surface of NP. In particular, protein corona constitute what the biological system actually sees when encounter the NP (Brun and Sicard–Roselli, 2014; Docter *et al.*, 2015b; Liu *et al.*, 2015; Serpooshan *et al.*, 2015; Caracciolo *et al.*, 2016) (Figure 2.1). Protein corona changes the interfacial properties of NP endowing it new identity termed biological identity which is significantly different from its synthetic identity. More specifically, protein corona transforms the synthetic identity of NP to biological identity, making the nanoparticle- protein corona complex to be seen as one entity (Monopoli *et al.*, 2012; Hadjidemetriou *et al.*, 2015; Maiolo *et al.*, 2015; Westmeier *et al.*, 2015; Bigdeli *et al.*, 2016).

This is the biological identity that mediate the interaction with membrane and biological barriers, determining the subsequent physiological responses including cellular uptake, kinetics, transport, biodistribution, signalling, and toxicity of the nanoparticles (Saptarshi *et al.*, 2013; Kelly *et al.*, 2015; Lee *et al.*, 2015; Mahmoudi *et al.*, 2015; Wan *et al.*, 2015; Kharazian *et al.*, 2016). Thus deep understanding of nanoparticle-protein corona complex and its biological implications is a vital step toward safe design of nanoparticle in medical application.

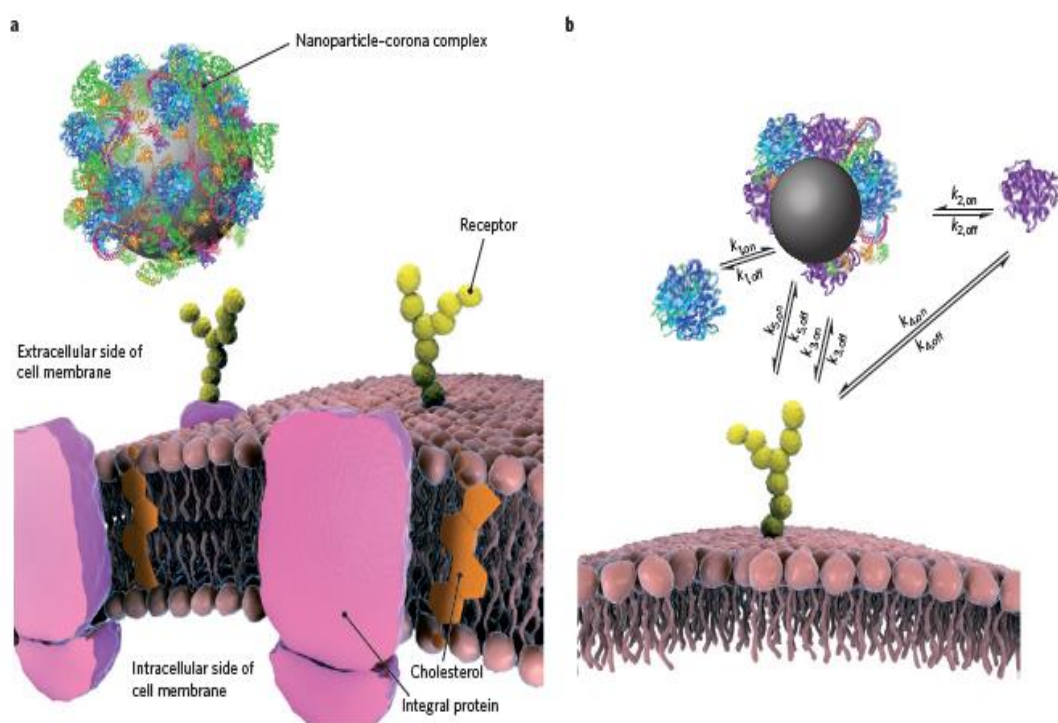


Figure 2.1: The nanoparticle–corona complex in a biological environment. (a) It is the nanoparticle–corona complex, rather than the bare nanoparticle, that interacts with biological machinery, here with a cell membrane receptor. (b) Relevant processes (arrows), in both directions (on/off), for a nanoparticle interacting with a receptor. Adapted from (Monopoli *et al.*, 2012).

2.2.1 Composition of the protein-corona

The identities of proteins in corona play a key role in defining the physiological response to NP- protein corona complex. Although, more than 3,700 proteins in the blood plasma compete for binding to the surface of nanoparticle, their abundance in the plasma is not related to their abundance in the protein corona. Furthermore, they are not merely those with the highest affinity for the surface of NP (Ge *et al.*, 2011; Martel *et al.*, 2011; Zhang *et al.*, 2011a; Dufort *et al.*, 2012; Monopoli *et al.*, 2012). It is noteworthy to mention that there is no universal protein corona for all nanoparticle and composition of protein corona is unique to each nanoparticle (Walkey and Chan, 2012).

Walkey and Chan established a trend in composition of protein corona by compiling a list of identified proteins for 63 nanomaterials across numerous studies. They have identified the total of 125 plasma proteins in protein coronas, demonstrating a subset of plasma proteins which adsorb at least to one nanomaterial, termed ‘adsorbome’. A similar trend was observed for all protein coronas in which 2 to 6 proteins for each nanomaterial were adsorbed abundantly, and other adsorbed proteins were low abundance proteins. The proteins that adsorb at high abundance to some nanomaterial are not the same abundant proteins to another. Some proteins may adsorb at high abundance to some nanomaterial but the same proteins adsorb on others with low abundance. They have classified adsorbed blood proteins to two groups; one is included of those proteins that have the capability to adsorb at high abundance to nanomaterial surface but it does not necessarily occur, and another one including of plasma proteins that can only adsorbed at low abundance (Walkey and Chan, 2012).

One protein group which has been extensively identified in protein corona of different nanoparticles is apolipoproteins. This protein which is part of lipoprotein complex, their main role is transporting lipids and cholesterol through the bloodstream (Lynch and Dawson, 2008; Monopoli *et al.*, 2012; Gunawan *et al.*, 2014). Adsorption of apolipoproteins on nanoparticles surface lead to interact with lipoprotein receptors on the cell surface (Wagner *et al.*, 2012; Saptarshi *et al.*, 2013; Tenzer *et al.*, 2013). This characteristic has been exploited to transport the drugs cross the blood–brain barrier (BBB), and reach the central nervous system (CNS) to treat CNS diseases such as Alzheimer's and Parkinson's diseases (Aggarwal *et al.*, 2009; Monopoli *et al.*, 2012; Walkey and Chan, 2012; Gunawan *et al.*, 2014).

Another group of protein that is often recognized in corona profile are complement proteins. This group of proteins are part of innate immune system that helps eliminating the pathogen from the body. The complement system which consist of more than 30 proteins tag the pathogen to be recognized by phagocyte (Tenzer *et al.*, 2011; Schöttler *et al.*, 2016). Fibrinogen another group of plasma proteins activate proinflammatory pathways and it is involved in the formation of blood clot (Deng *et al.*, 2011; Monopoli *et al.*, 2011a).

Immunoglobulins is another major component of plasma protein which play a key role in the immune system. This type of protein is consisting of five isotypes as follows, IgG, IgA, IgM, IgD, IgE. The smallest isotype of immunoglobulins, IgG is the only antibody that is able to across the placenta, and the biggest isotype IgM is the first antibody

that react to infection (Sacchetti *et al.*, 2013; Gunawan *et al.*, 2014). Aggarwal *et al.* has been reported that apolipoprotein, complement proteins, fibrinogen and immunoglobulins exist in the protein corona of almost any NP (Aggarwal *et al.*, 2009).

Adsorption of certain subset of proteins on the surface of nanoparticles enhance the uptake by macrophages cells of the reticuloendothelial system (RES). This category of proteins which is called opsonins is included of IgG, complement factors, and fibrinogen. Binding of opsonins to nanoparticles make a “molecular signature” for immune system, causing clearance from blood circulation and accumulation in the liver and spleen (Aggarwal *et al.*, 2009; Walkey and Chan, 2012; Pearson *et al.*, 2014b; Lee *et al.*, 2015).

Karmali and Simberg reviewed the identity of corona profile on different nanoparticles. They have concluded that on liposomes and polymeric nanoparticles, apolipoproteins are the main group of proteins that adsorb on the surface of nanoparticles, but this does not imply for inorganic nanoparticles. By reducing hydrophobicity of polymeric nanoparticles, the adsorption of ApoA-I, ApoA-IV, ApoC-III and ApoJ was decreased, while there was no change in the absorption level of IgG and albumin. Albumin had strong affinity for cationic lipoplexes and polyplexes as well as hydrophobic surfaces. The protein profile on hydrophilic inorganic nanoparticles significantly differ than polymeric nanoparticles with hydrophobic surface. Transferrin, haptoglobin, fetuin A, kininogen, histidine-rich glycoprotein, and clotting pathway factors were found on hydrophilic inorganic nanoparticles. Adsorption of complement C3 was increased by presence of hydroxyl group on nanoparticle surface (Karmali and Simberg, 2011).

2.2.2 Mechanisms and kinetics of protein adsorption

Protein corona forms through a dynamic process and adsorbed proteins are in constant state of flux. More specifically, protein corona is not a fix layer and proteins on NP surface are in continues exchange with free proteins in biological medium (Aggarwal *et al.*, 2009; Rahman *et al.*, 2013; Kharazian *et al.*, 2016). Formation of protein corona is a time dependent process which it evolves by the time. In particular, the composition of protein corona evolve considerably from what was formed at the initial stages due to ongoing exchange of high abundance protein which adsorb first with low abundance proteins adsorbing to nanoparticles surface afterward (Saptarshi *et al.*, 2013; Gunawan *et al.*, 2014; Wan *et al.*, 2015; Corbo *et al.*, 2016; Vilanova *et al.*, 2016).

The time evolution of protein corona formed around gold nanoparticles (AuNPs) in the cell culture media with 10% fetal bovine serum (FBS) was studied. The size of AuNPs were in the range of 4 to 40 nm and were stabilized with citrate ions, self-assembled monolayer (SAM) of mercaptoundecanoic acid (negative surface charge) and self-assembled monolayer (SAM) of aminoundecanethiol (positive surface charge). By increasing the incubation time, an enhancement in the hydrodynamic diameter, decrease in the surface charge and the red-shift of surface plasmon resonance was observed. This result indicates that the protein corona was evolved from a loosely weakly bound protein toward an irreversible persistent protein corona over time (Casals *et al.*, 2010).

The changes occurred over time in corona profile of lecithin-coated polystyrene nanosphere were investigated by Nagayama et al. In a liver perfusion study by employing

SDS-PAGE and western blotting the protein corona was analysed quantitatively and qualitatively in the time period of 5 to 360 minutes. Over time, an increment in the total amount of adsorbed proteins on nanoparticles surface was observed. Moreover, there were significant changes in the qualitative profile of protein in which complement C3 (C3) and immunoglobulin G (IgG) showed enhancement by the time and there was a slight increase in apolipoprotein E (ApoE) and immunoglobulin A (IgA). The hepatic uptake by liver macrophages (Kupffer cells) was higher over the time indicating increased opsonisation of NP (Nagayama *et al.*, 2007).

Protein corona evolves also as NP migrate from one biological compartment to another. The final corona retains the memory of its journey within the body. Thus, the composition of protein corona depends on all the environments which NP has passed through (Milani *et al.*, 2012; Monopoli *et al.*, 2012; Schleh *et al.*, 2012; Maiolo *et al.*, 2015). This concept can be employed to track the biodistribution of NP which in turn is important in nanotherapeutics applications (Gunawan *et al.*, 2014; Hamad-Schifferli, 2015; Schöttler *et al.*, 2016).

Lundqvist *et al.* studied protein corona evolution following moving from one biological fluid to another. They have simulated in vivo transport by incubating silica, polystyrene, and carboxyl-modified polystyrene NPs in human plasma following incubating the NPs in cytosolic fluid. The result showed remarkable evolution of the protein corona over time but the final corona after second incubation, encompasses the “fingerprint” of its history. They suggested that this phenomenon can be utilized to trace

the transport pathway of nanoparticle as well as the fate and biological behaviour of NP (Lundqvist *et al.*, 2011).

Recently, researchers are applying quantitative models to determine the associations between the structure of protein corona and distinctive protein corona 'fingerprints'. Chan *et al.* established a novel model to predict the biological behaviour of nanoparticle. They applied fingerprint of protein corona formed around 105 member library of surface-modified gold nanoparticles. They concluded that this model was 50% more accurate than previous model which utilize physicochemical properties of nanoparticle such as size, surface charge and aggregation state (Walkey *et al.*, 2014).

The rate of adsorption /desorption of proteins over time refers as kinetics of protein corona. Kinetics rate of each protein determine composition of protein corona at any given time. The possibility of the contact between nanoparticle-protein and probability of that contact lead to adsorption of protein defined by association constant (k_{on}). As such, dissociation constant (k_{off}) represent the binding energy of nanoparticle-protein complex, in which the higher the binding energy the lower the dissociation constant. The balance between association rates (k_{on}) and dissociation rate (k_{off}) of a protein is defined by binding constant (K_d) and indicates which proteins will be bound to the NP surface at equilibrium conditions. (Ehrenberg *et al.*, 2009; Dell'Orco *et al.*, 2010; Walkey and Chan, 2012; Mahmoudi *et al.*, 2013a; Del Pino *et al.*, 2014).

The dynamic process and evolution of proteins on the flat surface was analysed by Vroman at 1962 (Vroman, 1962). This researcher explained the complex series of proteins displacement by time known as “Vroman Effect” which has been applied to nano-surfaces as well. “Vroman Effect” states the identity of proteins adsorbed on the surface varies over time although, the total quantity of the adsorbed protein remains constant. (Jansch *et al.*, 2012; Vogler, 2012; Docter *et al.*, 2015a; Kharazian *et al.*, 2016). This phenomenon which depends on the abundance and affinity of the proteins along with their diffusion coefficients, is consist of two distinct stages refereed as ‘early’ and ‘late’ stage. During the early stage, adsorption of albumin, IgG, and fibrinogen take place which are highly motile proteins. These proteins will be then replaced by more static proteins such as apolipoproteins and coagulation factors during the late stage (Walkey and Chan, 2012; Rahman *et al.*, 2013). Kinetic study on solid lipid nanoparticles (SLN) showed that in the early stage albumin was adsorbed which was then replaced by fibrinogen. Over time IHRP (inter- α -trypsin inhibitor family heavy chain-related protein) and apolipoproteins substitute fibrinogen, indicating being in agreement with “Vroman effect”(Göppert and Müller, 2005).

Protein corona on nanoparticles are so thick to be considered as a monolayer of proteins but composed of multiple layers like Christmas tree structures (Walkey and Chan, 2012; Rahman *et al.*, 2013; Docter *et al.*, 2015a; Docter *et al.*, 2015b). Protein corona can be classified into two different types of protein layers, an inner layer which is consist of tightly bound proteins that they don’t readily desorb, termed “hard corona” and an outer layer comprise the loosely bound proteins, referred as “soft corona”. Hard corona represents proteins with high affinity and low-abundance which are characterized by slow

exchange rate with the biological medium. In contrast, soft corona represents proteins with low affinity and high-abundance characterized by rapid exchange rate with the biological medium (Tenzer *et al.*, 2013; Brun and Sicard–Roselli, 2014; Walkey *et al.*, 2014; Westmeier *et al.*, 2015; Zanganeh *et al.*, 2016).

Soft and hard corona can also be defined based on their residence time. Hard corona proteins have long residence time and they are more stable while soft corona proteins have short residence time and are more dynamic (Lynch and Dawson, 2008; Mahmoudi *et al.*, 2011a; Hadjidemetriou *et al.*, 2015). Due to their long lifetime on NP, hard corona resides on NP surface and undergo more biological process such as endocytosis. As such, hard corona plays more important role in determining the physiological response than soft corona (Nel *et al.*, 2009; Walczyk *et al.*, 2010).

In a model proposed by Cedervall *et al* protein corona was distinguished as fast and slow components. Fast component was formed in seconds around NIPAM/BAM nanoparticles whereas slow component was adsorbed within hours. Desorption pattern also indicated the same trend with lifetime of roughly 10 minutes for the fast component and almost 8 hours for the slow component (Cedervall *et al.*, 2007).

It is hypothesized that proteins in hard corona, interact directly with the NP surface, while proteins of the soft corona interact with proteins of hard corona through weak protein–protein interactions (Walkey and Chan, 2012; Polyak and Cordovez, 2016). A model has been suggested by Simberg *et al* in which protein corona is composed of “primary binders” and “secondary binders”. The former directly recognize nanoparticles

surface while the latter interact with the primary binders. The activity of primary binders might be altered by secondary binders as they are masked, leading to avoid interaction of primary binders with the biological medium (Simberg *et al.*, 2009).

2.2.3 Biological consequences of protein-corona formation on nanoparticles

Protein corona may affect numerous physiological responses such as toxicity, uptake, and biodistribution of nanoparticles. Formation of protein corona can be beneficial or disadvantageous in biomedical application of nanoparticles. Knowledge of implications of protein corona in clinical application of nanoparticles is of crucial importance to design the safe and applicable nanoparticles. Understanding the effect of protein corona on physiological responses enable preventing binding of certain proteins which stimulate phagocytosis and decrease blood circulation time of nanoparticle-based therapy. In the other hand, can make use of protein corona by designing nanoparticles to adsorb proteins of interest for targeting purpose which help directing of nanoparticle to the site of interest (Helou *et al.*, 2013; Sobczynski *et al.*, 2014; Lazarovits *et al.*, 2015; Mirshafiee *et al.*, 2016b).

Even though identical nanoparticles in different studies were applied, contradictory outcomes in cytotoxicity have been reported. Protein corona can affect toxicity profiles of nanoparticles in different ways. More specifically, protein corona may reduce NP-induced toxicities by acting as an interface in interactions with cell membrane and preventing cell membrane rupture (Corbo *et al.*, 2016). In absence of protein corona,

NP interact with cell membrane proteins directly and disrupt the integrity of cell membrane leading to cell death (Ruenraroengsak *et al.*, 2012; Wolfram *et al.*, 2014).

The impact of fetal bovine serum (FBS) driven protein corona on toxicity profile of Graphene Oxide (GO) nanosheets was evaluated. The cytotoxicity study at different concentration of FBS (1% and 10%) revealed that at low concentration (1%) cytotoxicity was in a concentration-dependent manner whereas by increasing serum concentration to 10% the cytotoxicity of nanoparticles was highly reduced. Moreover, it was shown that the cytotoxicity of GO nanosheets occurred due to direct interaction of GO nanosheets with cell membrane thereby causing the cell membrane undergone sever damage (Hu *et al.*, 2011b).

Due to negative charge of cell membrane the role of protein corona in reduction of toxicity can be more significant when NP is positively charged (Molinaro *et al.*, 2013; Wang *et al.*, 2013). Protein corona of positively charged polystyrene NPs was retained on nanoparticles surface as were taken up by cells and trafficked to lysosomes. In this compartment, corona coated NPs was degraded and lysosomal content was released. Hence, protein corona protected the cell from any damage caused by bare NPs till it was cleared through lysosome (Wang *et al.*, 2013).

Toxicity of protein corona coated carbon nanotubes CNTs on human acute monocytic leukemia cell line (THP-1) and human umbilical vein endothelial cells (HUVECs) were examined by Ge *et al.* It was found that protein corona significantly reduced toxicity of CNTs and as the density of adsorbed proteins increased, toxicity of

CNTs decreased (Ge *et al.*, 2011). Tenzer and co-workers studied the effect of protein corona on toxicity and pathophysiology of nanoparticles. It was found that pristine silica NPs triggered thrombocytes activation and caused hemolysis. whereas, protein corona formed on silica NPs inhibited these adverse effects and protected the cells from damage (Tenzer *et al.*, 2013).

In addition to protecting cell membrane, formation of protein corona on nanoparticle increase their stability which in turn mitigate toxicity. This is prominent specially for those nanoparticles which are not stable like quantum dots and their degradation leads to release of toxic product (Corbo *et al.*, 2016; Westmeier *et al.*, 2016). Moreover, toxicity of NPs can be associated to formation of reactive oxygen species (ROS) when NPs have semiconductor features. In this case, formation of protein corona prevents generation of ROS and increase the safety of NPs (Manke *et al.*, 2013; Minai *et al.*, 2013). Cytotoxicity of cobalt oxide on human monocytic cell line (THP-1) was examined by Casals, 2011. It was observed that following incubation with serum, toxicity profile of cobalt oxide was remarkably reduced due to decrease in ROS generation (Casals *et al.*, 2011). In another study, prior to exposure of ZnO NPs to human hepatocellular carcinoma (HepG2) cell, ZnO NPs pre incubated with cell culture medium. It was observed that the cytotoxicity of pre coated ZnO NPs were remarkably decreased to compare with pristine ZnO NPs. It was concluded that due to increase in amount and affinity of adsorbed proteins on NP surface, ROS formation as well as ZnO dissolution were inhibited leading to highly reduction of cytotoxicity (Yin *et al.*, 2015).

On the contrary, NP may cause denaturation in adsorbed proteins which can trigger toxicity. For instance, poly(acrylic) acid conjugated gold nanoparticles caused unfolding in the bound fibrinogen which in turn activated inflammatory signalling pathways result in release of inflammatory cytokines (Deng *et al.*, 2011). The correlation between formation of protein corona and cellular uptake has been established. The nature of adsorbed plasma proteins is a determinant factor in degree and rate of cellular uptake (Laurent *et al.*, 2013; Lee *et al.*, 2015; Maiolo *et al.*, 2015; Westmeier *et al.*, 2015). More specifically, a subset of plasma proteins called “opsonin” which includes immunoglobulins and complement proteins enhance the cellular uptake while another subset of plasma protein referred as “dysopsonins” such as albumin lowers the uptake level (Owens and Peppas, 2006; Moghimi *et al.*, 2011; Walkey and Chan, 2012). In some cases, protein corona diminishes nanoparticles adherence to the cell membrane result in reduction of uptake (Lesniak *et al.*, 2012; Smith *et al.*, 2012; Wolfram *et al.*, 2014).

The role of presence of protein corona on silica nanoparticles uptake by A549 lung epithelial cells was investigated. It was reported that the same nanoparticles show different biological responses depends on presence or absence of protein corona. In particular, in the absence of protein corona due to stronger adhesion of silica nanoparticles to the cell membrane higher internalization efficiency was observed (Lesniak *et al.*, 2012). Oligonucleotide-functionalized gold nanoparticles (DNA-Au NPs or siRNA-Au NPs) were shown to have higher uptake in serum-free medium by HeLa cells. Pharmacological methods revealed that the serum proteins impaired the adhesion of nanoparticles to membrane of Hela cells (Patel *et al.*, 2010).

The uptake of dihydrolipoic acid-coated quantum dots (DHLA-QDs) by HeLa cells were studied by Treuel and co-workers. It was observed that following formation of protein corona on nanoparticles surface the uptake level has substantially decreased (Treuel *et al.*, 2014). Using carboxyl functionalized Iron platinum (FePt NPs), it was shown that after exposure to human transferrin the uptake of these nanoparticles by HeLa cells was highly reduced (Jiang *et al.*, 2010). Wang *et al.* investigated uptake of Gold nanoparticles (AuNPs, 20 nm) by mouse myogenic (Sol8) cells in presence and absence of protein corona. It was shown that presence of protein corona suppress the nanoparticles to be taken up by mouse myogenic cells (Wang *et al.*, 2012).

On the contrary, some other researches indicated that protein corona facilitate uptake of particles by cells. The contradictory results may be due to different types of uptake that take place by cell such as specific or non-specific cellular uptake. Specific uptake is mediated by membrane receptors and have been reported to increase in presence of protein corona whereas, non-specific cellular uptake is regardless of cell receptors and is a random process which decrease with formation of protein corona (Brun and Sicard–Roselli, 2014; Schöttler *et al.*, 2016). The impact of presence of protein corona on degree of specific uptake was assessed by Kraiss, *et al.*, 2014. Uptake study of folic acid-functionalized iron oxide nanoparticles by ovarian cancer cells revealed that existence of protein corona is a requisite for uptake of nanoparticles (Kraiss *et al.*, 2014). Using titanium dioxide (TiO₂) nanoparticles, uptake of these particles by A549 and H1299 human lung cell lines after incubation with fetal bovine serum (FBS) were evaluated. It was shown that formation of protein corona increased the level and rate of nanoparticles uptake (Tedja *et al.*, 2012a).

In addition, employing different cell lines in uptake studies may demonstrate contrasting results. While protein corona suppress uptake of nanoparticles by monocytes due to blocking the surface of nanoparticle, some cells such as macrophages, neutrophils, and dendritic cells express receptors on their surface that enable them to interact with opsonins in protein corona result in triggering internalization (Karmali and Simberg, 2011; Goodridge *et al.*, 2012; Wolfram *et al.*, 2014; Corbo *et al.*, 2016). Effect of different cell lines on uptake of nanoparticles in presence of protein corona was investigated by Yan *et al.* Uptake of disulfide-stabilized poly (methacrylic acid) nanoporous polymer particles (PMA_{SH} NPPs) by monocytes and macrophages was compared. Monocytic cells, THP-1 internalized nanoparticles much fewer following formation of protein corona than bare nanoparticles. Uptake of nanoparticles by differentiated macrophage-like cells (dTHP-1) has shown an increment compared to bare nanoparticles due to trigger of scavenger receptors (Yan *et al.*, 2013).

2.3 Cellular uptake pathways of NPs

Cell membrane (CM) employs different mechanisms to exchange substances which are mainly divided into two categories: passive transport and active transport. Gases such as oxygen and carbon dioxide, hydrophobic molecules such as benzene and uncharged molecules such as water and ethanol diffuse across the membrane from the regions of higher to lower concentration. This kind of transport which is along the concentration gradient and occurs without assistance of energy is called passive transport. In contrast, active transport occurs against the concentration gradient by using energy which is provided by adenosine triphosphate (ATP) (Feher, 2012; Backes, 2015; Douglas

et al., 2015). Polar or charged biomolecules that cannot pass through the hydrophobic plasma membrane are internalized by a form of active transport which is called endocytosis. In this process, the cell engulfs the materials inside the extracellular fluid by invagination of CM and buds off inside the cell, forming a membrane-bounded vesicle called an endosome (Makaraci and Kim, 2018).

Endocytosis can be basically classified into two major categories: phagocytosis and pinocytosis. Phagocytosis (cell eating) is the process of taking in debris, bacteria or other large size solutes by specialized mammalian cells called phagocytes (i.e. monocytes, macrophages and neutrophils) (Nazario-Toole and Wu, 2017; Rajendran *et al.*, 2018). Integral to phagocytosis is a process called opsonization by which opsonins such as immunoglobulins and complement proteins coat the target materials to trigger the phagocytes of their presence and to initialize phagocytic activity (Xiang *et al.*, 2012). As the phagocyte begins to ingest the target material, it will simultaneously stimulate the formation of a membrane-bound vesicle called phagosome into which the ingested materials are compartmentalized within the phagocyte. At the latter stages of this process, the phagosome will fuse with the lysosome and the materials are digested at acidic pH by the hydrolytic enzymes contained within the lysosomal lumen (Hillaireau and Couvreur, 2009; Xiang *et al.*, 2012).

In all cell types, small particles within the range of nanometers are internalized by pinocytosis (Zhao *et al.*, 2011). In pinocytosis, “cellular drinking” plasma membrane